FOREX Publication
Open Access | Rapid and quality publishing

International Journal of
Electrical and Electronics Research (IJEER)
Research Article | Volume 13, Issue 2 | Pages 325-336 | e-ISSN: 2347-470X

Optimized Fuzzy SVM with Chaotic Henry Gas Solubility Algorithm for Fault Identification in Rotating Machinery

Dr. Mohan S B[1], Dr. Prajith Prabhakar[2*], Dr. Yokesh V[3], M Bharathi[4], Dr. Gayathry S Warrier[5], and Dr Mahalakshmi J[6]

[1]*Associate Professor, Department Of ECE, S A Engineering College, Chennai, India; drsbmohan@gmail.com*
[2]*Department of Smart Materials, Saveetha School of Engineering, Saveetha Institute of Medical and Technical Science, Chennai, India; prajithprabhakar15@gmail.com*
[3]*Department of Electronics and Communication Engineering, Sathyabama Institute of Science and Technology, Chennai, India; yokesh.inba@gmail.com*
[4]*Assistant Professor, Department of Electronics and Communication Engineering, Jeppiaar Institute of Technology, Sriperumbudur, India; bharathimjbn@gmail.com*
[5]*Assistant Professor, Department of Computer Science, Christ University Bangalore, Karnataka, India; gayathry.warrier@christuniversity.in*
[6]*Assistant Professor, Department of Computer Science, Christ University Bangalore, Karnataka, India; mahalakshmi.j@christuniversity.in*

***Correspondence:** *Dr. Prajith Prabhakar; Email: prajithprabhakar15@gmail.com*

ABSTRACT- Reliable and accurate fault diagnosis in rotating machinery is vital for minimizing unplanned downtime, reducing maintenance costs, and ensuring operational safety in industrial environments. Traditional diagnostic approaches depend heavily on manual feature extraction from vibration signals, which can be time-consuming, expertise-dependent, and prone to missing subtle fault patterns. This study presents a novel hybrid framework—**IDL-OFSVM**—that combines **Intelligent Deep Learning (IDL)** with an **Optimized Fuzzy Support Vector Machine (OFSVM)** for automated fault classification. Vibration signals are first transformed using the Continuous Wavelet Transform (CWT), and deep features are extracted via the lightweight MobileNet architecture. The **Chaotic Henry Gas Solubility Optimization (CHGSO)** algorithm significantly enhances the classification model's performance, which effectively tunes the FSVM parameters. Experimental evaluations on benchmark datasets show that the proposed method achieves 99.8% training and 99.7% testing accuracy, outperforming several state-of-the-art approaches. Beyond technical accuracy, the framework offers practical advantages, including reduced dependency on domain expertise, suitability for real-time monitoring, and potential integration into predictive maintenance systems. These benefits make the IDL-OFSVM model a promising solution for industrial fault diagnosis applications, where reliability, speed, and scalability are crucial.

Keywords: Fault diagnosis, Rotating machinery, Fuzzy Support Vector Machines, Parameter tuning, Vibration signals, Fuzzy logic.

ARTICLE INFORMATION

Author(s): Dr. Mohan S B, Dr. Prajith Prabhakar, Dr. Yokesh V, M Bharathi, Dr. Gayathry S Warrier, and Dr Mahalakshmi J;
Received: 15/02/2025; **Accepted**: 06/06/2025; **Published**: 30/06/2025;
E- ISSN: 2347-470X;
Paper Id: IJEER 1502-07;
Citation: 10.37391/ijeer.130217
Webpage-link:
https://ijeer.forexjournal.co.in/archive/volume-13/ijeer-130217.html

1. INTRODUCTION

Big generator sets, new supersonic vector aviation engines, high-performance marine propulsion motors, precise machine tool spindles, and other strong rotating gear have rapidly expanded in the past year, heading towards ultrahigh speed and automation [1,2]. Reliability and safety in rotating machine operations depend on a well-designed system for detecting and fixing problems and keeping tabs on their health [3]. In this context, fault diagnosis has become a critical concern, especially as rotating machinery becomes more complex and data-rich. Emerging micro-fault monitoring and diagnostic tools are the focus of heavy research among faulty diagnostic researchers. The cutting arms' early fault detection and identification (IFDI) is an essential assurance for a road header's efficient functioning. The data analysis tools should be optimized efficiently, and the fault diagnostic approach is restricted in its applicability due to a lack of fault samples [4,5]. Methods for identifying defects can be either data-driven or mechanism-analytical. Software solutions designed specifically for data collection, management, and display are known as data-driven systems and apps. Just like any other type of package, these systems are usually built using software development tools, technologies, and methods. Instead of a list of to-dos needing approval, data-driven programming describes the data that must be coordinated and the distribution that must occur through program declarations. These are data-driven languages because the data is an arrangement of lines in an input stream.

FOREX Publication
Open Access | Rapid and quality publishing
International Journal of Electrical and Electronics Research (IJEER)
Research Article | Volume 13, Issue 2 | Pages 325-336 | e-ISSN: 2347-470X

Also, these languages are referred to as line-oriented languages, and regular expressions or line numbers are usually used for pattern matching.

Analytics is a computer-assisted method of systematically reviewing statistical or data sets. Its goal is to find, understand, and explain meaningful patterns in data. It also involves using data trends to make informed judgments. When dealing with massive amounts of data, analytics can really shine. It uses statistics, code, and operations research to find out how things work [6].

Despite their advantages, many deep learning (DL) models like autoencoders suffer from input sensitivity and require substantial tuning effort. Moreover, output improvement is not always guaranteed, and performance inconsistencies persist. This research presents a novel Chaotic Henry Gas Solubility Optimization (CHGSO) method intending to restore the solution's accuracy. Using the mean fitness rate and standard deviation, the planned irregular is validated on 47 standard challenges of different modalities, including multimodal, secure measurement multimodal, and unimodal. According to the untested results, the proposed approach performs better than the existing method [31-32].

To address the restraints in precision and generalization of conventional FSVM and DL approaches, this work integrates MobileNet—a lightweight deep learning model—with an optimized fuzzy SVM classifier. While this method does produce ideal results, building a complex scheme with higher precision is challenging. Using the decoding module to fix related but separate problems is also a pain. Many pieces of rotating machinery and equipment now use new data-collecting technology and smart sensors, thanks to the proliferation of the "Internet+" and the Internet of Things [7, 8].

There are several documented analysis techniques, such as Principal Component Analysis (PCA), Empirical Mode Decomposition (EMD), Wavelet Transform (WT), Hilbert–Huang transforms, Wigner-Ville distribution, decision tree, order tracking, and rough sets theory, among others. Recently, EMD has been proposed for nonlinear and non-stationary signals. EMD decomposes signals into Intrinsic Mode Functions (IMFs) based on local temporal features, offering high adaptability. The Wavelet Transform generalizes the STFT and transforms signals into wavelet-like basis functions. These routines make frequency-domain localization possible by computing a scaled wavelet signal convolution.

By highlighting similar and dissimilar data patterns, PCA can help identify data trends and reduce dimensionality while maintaining variance. Unlike fixed-basis methods, the Hilbert–Huang Transform (HHT) is another nonlinear, non-stationary signal processing algorithm that uses EMD for adaptive decomposition. The Wigner distribution (WD) is unique among linear time-frequency representations.

Decision trees allow intuitive visualization of choices and outcomes, while rough set theory helps deal with imprecise or noisy datasets by constructing equivalence classes and discretizing continuous features. Among these, Wavelet Transform (WT) has been especially effective in fault detection due to its dual localization in time and frequency domains [9, 10]. It is frequently used alongside advanced techniques like SVR, Genetic Algorithms (GAs), and Support Vector Machines (SVMs) [11].

Recently, Deep Learning (DL) has gained traction in fault diagnostics. Traditional models like SVM are limited in handling complex, high-dimensional input [12]. DL models such as CNN, Deep Belief Networks (DBN), and Stacked Autoencoders (SAE) have shown promise. SAE and DBN utilize unsupervised pretraining, while CNNs excel at spatial feature extraction due to their convolution and pooling layers [13]. Their shared-weight architecture makes them computationally efficient. Hybrid models that integrate deep learning (DL) with Support Vector Machines (SVM) or Fuzzy Support Vector Machines (FSVM) have potential in defect diagnostic tasks; nonetheless, they are constrained by many restrictions that hinder their practical implementation. Primarily, most deep learning architectures employed in these models, such as VGG and ResNet, are computationally intensive, rendering them inappropriate for real-time implementation on edge or embedded devices often utilized in industrial settings.

Secondly, while FSVM incorporates fuzzy logic to manage uncertain and noisy data, its efficacy is frequently limited by the necessity for manual adjustment of fuzzy membership functions and kernel parameters, potentially resulting in inferior classification outcomes. Moreover, these models frequently exhibit sensitivity to outliers and may lack generalizability when trained on limited or unbalanced datasets, a prevalent situation in industrial defect identification. Moreover, conventional optimization techniques employed with FSVM, such as grid search or rudimentary metaheuristics, frequently encounter difficulties in effectively navigating the intricate parameter space, leading to prolonged training durations and convergence to local minima. These constraints underscore the necessity for a more effective, streamlined, and resilient methodology for fault classification in rotating machinery.

However, most existing hybrid models lack integration of both lightweight and high-precision mechanisms. Hence, this paper proposes a MobileNet-based deep feature extractor coupled with an FSVM classifier optimized using CHGSO to address the dual challenge of computational efficiency and high diagnostic accuracy.

2. EARLIER MECHANICAL FAULT DIAGNOSIS APPROACHES

Modern methods for fault diagnostics that use DL models are discussed in this section. A novel responsibility judgement method with three main steps was introduced by Chen et al. [14]. The method uses CNN and ELM. Finding preprocessed representations of the raw shaking indication is the first step in using the CWT. The following phase is building a convolutional neural network (CNN) using a square pooling architecture to extract more complex information. This approach could cut

FOREX Publication
Open Access | Rapid and quality publishing
International Journal of Electrical and Electronics Research (IJEER)
Research Article | Volume 13, Issue 2 | Pages 325-336 | e-ISSN: 2347-470X

computing costs in half since it does not need fine-tuning or extra training. Finally, ELM is used as a trustworthy classifier to improve the diagnostic architecture's classification ability. However, a key constraint in this hybrid architecture lies in the lack of adaptive learning in ELM, making it less effective in capturing non-stationary fault characteristics than more robust classifiers like SVM.

Guo et al. [15] created a novel diagnostic method utilizing CNN to classify CWTS directly. Gong et al. [16] presented a new method, an enhanced CNN-SVM strategy. Combining SVM with the global average pooling method enhances the conventional CNN module. Nevertheless, the fusion strategy lacks end-to-end optimization, potentially causing feature misalignment and suboptimal learning during backpropagation. Improved classification accuracy was suggested by Kolar et al. [17] using a three-axis accelerometer signal as an input to a deep learning layer. The layer would then manually remove signal properties, making it a higher-definition simplified replica of the original. An LSVM method (SVM) is employed for attribute classification. Using the collected photos, simulations have been executed. Using a support vector machine (SVM) classifier in conjunction with fractal and power spectral properties, Kolar et al. correctly identified thirty retinal fundus images (74% accuracy).

Jiang et al. [18] developed an endwise diagnostics approach or intelligent defect detection method based on 1D-CNN. In particular, the module supplies the unprocessed vibration signals to identify them. Subsequently, a balanced dataset is created using a data expansion approach known as 1D-DCGAN, which combines CNN and generative adversarial networks to produce tiny-size fault samples. However, while 1D-CNN combined with GANs introduces data diversity, it still lacks the decision boundary optimization capabilities offered by SVM-based models, limiting generalization on real-world imbalanced datasets.

Wu et al. [19] suggested a hybrid classification AE approach as a method for fault diagnosis. Using a SoftMax classifier based on AE-prepared information, this recently aimed to diagnose the healthcare situation directly. To simultaneously make the module proficient with unlabeled and labelled data, the widely used MSE of unsupervised AE is modified to control the information tags. When combined with the SoftMax classifier, it could be effective. Feet concentration needs to be raised to classify photos within the same group, even if the traditional SoftMax classifier can classify features into numerous categories. Consequently, there is room for improvement in the ultrasonic task of using a machine-learning system to identify similar signal waveforms. Conventional wisdom holds that a SoftMax classifier's efficacy can be gauged by comparing its classification accuracy to the rate at which the harm purpose is met. In contrast, the proposed model integrates DL feature extraction with FSVM's capacity for margin maximization, thus overcoming SoftMax's shortcomings in class separation and contributing to improved classification robustness.

Lastly, with the help of the gathered features, the training method is designed to represent the scenario at each level visually. Following manual maintenance operations, Souza et al. [20] suggested utilizing PdM-CNN for defect classification in spinning equipment. Examining the practical applications of this research, this study follows a systematic approach that encompasses data preparation, feature engineering, model selection, and performance assessment. Utilizing an artificial dataset, we demonstrate the efficacy of Support Vector Machines (SVM) and Convolutional Neural Networks (CNN) in detecting malfunctions in rotating machinery [21]. In six cases, one is normal, and five are defective; thermal pictures of rolling element bearings are considered. Subsequently, a classification efficiency-based similarity is developed using shallow and DL approaches that incorporate ANN and CNN. Nonetheless, these approaches rely on domain-specific feature preprocessing, whereas the proposed hybrid model demonstrates greater adaptability and minimal pre-engineering dependency. A new method utilizing NSTAE optimization with PSO was shown by Haidong et al. [22].

3. PROPOSED MODEL

This method incorporates a new IDL-OFSVM to identify and classify rotating machine problems. The proposed IDL-OFSVM includes preprocessing, MobileNet-based feature extraction, FSVM-based classification, and CHGSO-based parameter tweaking. Figure 1 depicts the workflow of the IDL-OFSVM approach, and the modules depicted in the picture are addressed briefly in the following subsections.

3.1. Data Preprocessing

It is a process with a specific rotational load and speed. To detect faults in various operational situations, tremor signs from the mechanism in the overall load and speed variety must be obtained for training [15]. The vibration signals are made up of rotating speed data to remove this control. Notably, while the equipment is in constant function, the rotating speed in the trained samples is deemed constant.

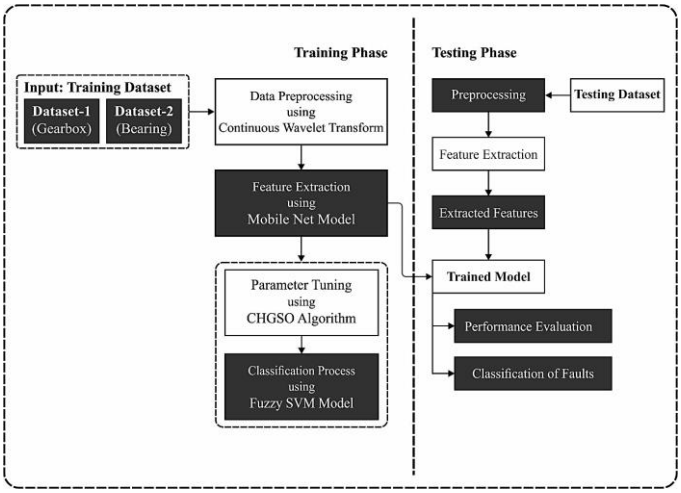

Figure 1. Overall process of IDL-OFSVM model

CWT created the localization design of STFT. A CWT is utilized to sign period regularity processing and diagnoses. A CWT of $x(t)$ is defined as the convolution of the signal $x(t)$

FOREX Publication
Open Access | Rapid and quality publishing
International Journal of Electrical and Electronics Research (IJEER)
Research Article | Volume 13, Issue 2 | Pages 325-336 | e-ISSN: 2347-470X

using wavelet function $\Psi_{a,b}(t)$. The data series is first processed using the discrete Fourier transform before being used to compute the CWT spectrum. For each scale (specified frequency) in the spectrum, the frequency response of the daughter wavelet is then determined analytically. The CWT is used in this system to decompose data from 1 to l, where l is frequently superior/equivalent to *2q*:

$$C_a(k) = \int_1^{2q} x\,(t) \cdot \overline{\Psi}_{a,b}(t)dt \qquad (1)$$

$C_a(a = 1,2,3, \dots, l)$ denotes the wavelet coefficient of $x(t)$ in ath scale and $\overline{\Psi}_{a,b}(t)$ represents the complex conjugate solution of the ripple procedure at conversion b and grading a. The CWT generates the coefficient on many sections of the indication with different scaling issues. A 2-dimensional copy using this wavelet coefficient immediately displays an indication in period incidence fields.

Attaining each wavelet coefficient in $P = [C_1, C_2, \dots, C_l]$, it is altered into a gray matrix P_{new} as:

$$P_{new}(i,j) = \left[\frac{P(i,j)-p_{min}}{p_{max}-p_{min}} \times 255 + \frac{1}{2}\right] \qquad (2)$$

$Whereas\ max\ and\ pain$ denote the maximal and minimal components of P. A value of the element in P_{new} denotes the gray values in the sequence from zero to 255. So, P_{new} represents the CWTS of the novel signal.

3.2. Feature Extraction: Mobile Net Architecture

The MobileNet network is being developed to improve the real-world efficacy of DL in hardware constraints. This network could reduce the number of variables while maintaining accuracy. Previous research has shown that MobileNet requires 1/33 of the variables of VGG16 to achieve comparable classification accuracy in the ImageNet1000 classification challenge. The convolutional framework of MobileNet is depicted in *figure 2*. Pw, Cw and Conv denote a deep and separable convolutional framework. It can be divided into two layers: pointwise (Pw) and depthwise (Dw). Depthwise convolution, also known as spatial convolution, is a type of spatial convolution in which each channel of an input is processed independently. When performing a 1x1 convolution on the depthwise convolution output channels, you project the channels onto a new space. The activation function ReLU and the BN technique process all convolutional results. The activation in this form of the rectified linear unit is limited to a maximum size. This is because its robustness is increased when used with low-precision calculations. PyTorch provided the image. The source of this information is MobileNets: Effectual Convolutional Neural Networks for Mobile Vision Applications. RELU6 is a popular activation function employed in deep convolutional neural networks. It is frequently found in mobile machine learning instances because it is used in Google's optimized MobileNet architecture and would cause issues if converted to run on a mobile device.

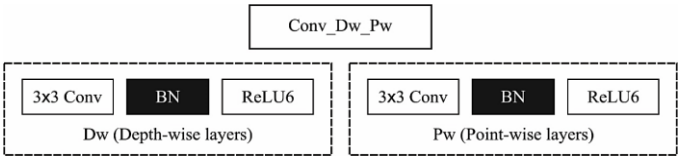

Figure 2. Basic structure of MobileNet

In this study, the beginning purpose of ReLU is substituted with ReLU6, and the standardization is carried out using the BN approach, which aids in the adaptation of automatic data distribution. The activating role of ReLU6 is proven by:

$$y = min(max(z, 0), 6) \qquad (3)$$

Meanwhile, z denotes the value of each pixel in the element map.

MobileNet's cavernous and separable convolution framework expedites the trained dataset and drastically minimizes the calculations needed. The following is the reason: The regular convolutional framework is represented by,

$$G_N = \sum_M^N K_{M,N} * F_M \qquad (4)$$

whereas $K_{M,N}$ denotes the filter, $and\ N$ and M correspondingly signify the quantity of contribution and production stations. In the regular convolutional, the input images, comprising the feature images, F_M denotes the input image, comprising a feature map that utilizes the fill style of zero paddings [23]. *Figure 3* shows the different layers in the MobileNet method.

Type / Stride	Filter Shape	Input Size
Conv / s2	3 x 3 x 3 x 32	224 x 224 x 3
Conv dw / s1	3 x 3 x 32 dw	112 x 112 x 32
Conv / s1	1 x 1 x 32 x 64	112 x 112 x 32
Conv dw / s2	3 x 3 x 64 dw	112 x 112 x 64
Conv / s1	1 x 1 x 64 x 128	56 x 56 x 64
Conv dw / s1	3 x 3 x 128 dw	56 x 56 x 128
Conv / s1	1 x 1 x 128 x 128	56 x 56 x 128
Conv dw / s2	3 x 3 x 128 dw	56 x 56 x 128
Conv / s1	1 x 1 x 128 x 256	28 x 28 x 128
Conv dw / s2	3 x 3 x 256 dw	28 x 28 x 256
Conv / s1	1 x 1 x 256 x 256	28 x 28 x 256
Conv dw / s1	3 x 3 x 256 dw	28 x 28 x 256
Conv / s1	1 x 1 x 256 x 512	14 x 14 x 256
5 x Conv dw / s1	3 x 3 x 512 dw	14 x 14 x 512
5 x Conv / s1	1 x 1 x 512 x 512	14 x 14 x 512
Conv dw / s2	3 x 3 x 512 dw	14 x 14 x 512
Conv / s1	1 x 1 x 512 x 1024	7 x 7 x 512
Conv dw / s2	3 x 3 x 1024 dw	7 x 7 x 1024
Conv / s1	1 x 1 x 1024 x 1024	7 x 7 x 1024
Avg Pool / s1	Pool 7 x 7	7 x 7 x 1024
FC / s1	1024 x 7	1 x 1 x 1024
GNB, SVM / s1	Classifier	1 x 1 x 7

Figure 3. Layers in MobileNet Model

FOREX Publication
Open Access | Rapid and quality publishing
International Journal of Electrical and Electronics Research (IJEER)
Research Article | Volume 13, Issue 2 | Pages 325-336 | e-ISSN: 2347-470X

If the size and channel of input images denote $D_F * D_F$ and M, respectively, it is essential to have N strainers using M networks with the size $D_K * D_K$ before resulting in N feature images of size $D_K * D_K$. The computation cost is $D_K * D_K * M * N * D_F * D_F$.

In contrast, the Dw equation is given by,

$$`G = \sum_M^N \grave{K}_{1,M} * F_M \quad (5)$$

whereas $\grave{K}_{1,M}$ denotes the filter. If the period extent is one, zero fillers ensure that the extent of the characteristic graph remains constant following the application of the deep and separable convolution framework. The deep separable convolutional framework of MobileNet could attain a similar output as regular convolutional built on similar inputs. The Dw stage requires M filters with one channel with the size $D_K * D_K$. The Pw stage requires $an\ N$ filter using $an\ M$ channel of 1×1. In this instance, the computation cost of the deep separable convolutional framework represents $D_K * D_K * M * D_F * D_F + M * N * D_F * D_F$, around $N1 + \frac{1}{D_K^2}$ as regular convolution.

Compared to the conventional normal distribution, the BN technique modifies the data by specifying two learning factors, avoiding gradient disappearance, and modifying challenging variables (for example, dropout ratio and learning rate).

3.3. Design of OFSVM Model for Classification

The retrieved characteristics from the previous stage are input into the OFSVM during the classification phase. The SVM is a boundary-founded organization technique in which an ideal hyperplane can split distinct courses as long as the structural risk minimization criteria are followed. Furthermore, SVM can detect novelty [24]. Assume that the training dataset $T = \{(x_1, y_1), (x_2, y_2), \dots, (x_n, yn)\}$, in which $x_i \in R^p, i = 1,2, \dots, n$ denotes the feature trajectory and $y_i \in \{-1, +1\}, i = 1,2, \dots, n$ represents the respective binary reply.

$$\min_{\alpha} \tfrac{1}{2} \sum_i^N \sum_{j=1}^n \alpha_i \alpha_j y_i y_j \, K(x_i, x_j) - \sum_{i=1}^n \alpha_i \, s.t. \sum_{i=1}^n \alpha_i y_i =$$

$$0,0 \le \alpha_i \le C \quad (6)$$

Whereas $\alpha_i (1 \le i \le N)$ represents the Lagrange multiplier equivalent to the sample x_i, $K(\cdot\cdot)$ indicates the kernel function, and C signifies the penalty variable, determining the trade-off between minimizing misclassification error and increasing classification margin. By overcoming the optimization challenges in *eq. (6)*, it is possible to achieve the following:

$$D(x) = sign[\sum_{i=1}^N \alpha_i \, y_i K(x_i, x) + \mathrm{b}] \quad (7)$$

In traditional SVM, each data point is considered equally important, and the objective function allocates the punitive parameter. However, in some real-time classification applications, sample points, such as noises/outliers, may need to be correctly assigned to each class. Not all sample points have an identical meaning to the decision surface. The notion of fuzzy SVM (FSVM) is employed to solve this problem. Because all sample points have fuzzy membership, distinct samples may contribute to the decision surface differently.

$$S = \{(x_1, y_i, s_i), i = 1, \dots, N\} \quad (8)$$

Where which $x_1 \in R^n$ denotes the n-dimension sample point, $y_i \in \{-1, +1\}$ signifies its class label, and $s_i (i = 1, \dots, N)$ implies a fuzzy membership that fulfills $\sigma \le s_i \le 1$ using a sufficiently small constant $\sigma > 0$. $\Re$ quadratic optimization problem for classification is given below.

$$\min_{w, s, \xi_i} \tfrac{1}{2} w^T w + C \sum_{i-1}^l s_i \, \xi_i \quad (9)$$

$$s.t. \, y_i (w^T x_l + b) \ge 1 - \xi_i, \xi_i \ge 0, i = 1, \dots, l,$$

whereas w indicates a standard vector of the hyperplane, b indicates a bias term, and C characterizes a parameter that manages the trade-offs amongst the costs of classification margin and misclassification error [25]. As s_i denotes the attitude of the respective point x_1 to one class and the slack parameter ξ_i symbolizes a measure of error, later, the $s_i \xi_i$ is used to measure the error with dissimilar weights. The higher the s_i, the more strongly the relevant points are processed, whereas the lower the s_i, the less significantly the respective points are processed.

For solving the FSM problem, eq. (9) is transformed into the binary problem by providing LaGrange multipliers α_i:

$$max \sum_{i=1}^N \alpha_i - \tfrac{1}{2} \sum_{i=1}^N \sum_{j=1}^N \alpha_i \, \alpha_j y_i y_j x_i x_j \quad (10)$$

$$s.t. \sum_{i=1}^N y_i \, \alpha_i = 0, 0 \le \alpha_i \le s_i C, i = 1, \dots, N.$$

By resolving these dual problems in *eq. (10)*, we get an optimum $\alpha_i . Similarly, w$ and b could be obtained by the regular SVM. The CHGSO model is used to optimally adjust the weight and bias variables of the OFSVM, hence improving the classification result. Solubility refers to the ability of many solutes to melt in an exact amount of flush at a specific pressure and temperature using Henry's law. As a result, the application of Henry's law stimulates the HGSO. It can be used to describe the solubility of a less soluble gas in a liquid. [26]. When it comes to pressure, increasing the pressure improves gas solubility. It might be proven scientifically as follows.

***Step 1*:** The population size N and position of gas is given by:

$$X_i(t+1) = X_{minm} + r \times (X_{maxm} - X_{minm}) \quad (11)$$

Whereas, Xi(t+1) refers to the position of the ith gas molecule, the position of i^{th} gas in the populace N is indicated in $X_{(i)}$, r signifies arbitrary quantity between 0 and 1. X_{minm}, X_{maxm} signifies the boundary values, and t indicates iteration time [29-30]. Henry constant of type $\left(H_j(t)\right)$, a quantity of gas i, incomplete heaviness $P_{i,j}$ of gas i in the collection j, and $\nabla_{sol} \, E/R$ constant rate of category $j(C_i)$ is begun.

FOREX Publication
Open Access | Rapid and quality publishing
International Journal of Electrical and Electronics Research (IJEER)
Research Article | Volume 13, Issue 2 | Pages 325-336 | e-ISSN: 2347-470X

$H_j(t) = l_1 \times rand(0,1), P_{i,j} = l_2 \times rand(0,1), C_j = l_3 \times rand(0,1)$ (12)

Whereas Hj(t) is the Henry's constant for gas type j,$P_{i,j}$ is partial pressure and j is the constant rate, l_1, l_2, l_3 denotes the constant values.

***Step 2*:** The population agent is split into equal clusters equivalent to the quantity of gas. All the clusters contain similar gas and Henry's constant values (H_j).

***Step 3*:** Evaluation. To locate the best gas, all of the cluster j is estimated. The gas is then assessed in order to produce the best possible gas.

***Step 4*:** Upgrade the Henry $coefficient$ as follows.

$H_j(t+1) = H_j(t) \times exp\left(-C_j \times \left(1/T(t) - 1/T^{\theta}\right)\right), T(t) = exp(-t/iter)$ (13)

Whereas T (t) is a temperature decay function, H_j denotes Henry's constant for group j, T signifies temperature T^{θ} signifies continuous and corresponds to 298.15, and iter represents the general number of iterations.

***Step 5*:** Upgrading solubility as follows.

$$S_{i,j}(t) = K \times H_j(t+1) \times P_{i,j}(t) \quad (14)$$

$S_{i,j}(t)$ is the solubility of gas *i* in group *j* at time *t*.

***Step 6*:** Upgrading location as follows:

$$X_{i,j}(t+1) = X_{i,j}(t) + F \times r \times \gamma \times \left(X_{i,best}(t) - X_{i,j}(t)\right) + F \times r \times \alpha \times \left(S_{i,j}(t) \times X_{best}(t) - X_{i,j}(t)\right)$$
$$\gamma = \beta \times exp\left(\frac{-F_{best}(t)+\varepsilon}{F_{i,j}(t)+\varepsilon}\right), \varepsilon = 0.05 \quad (15)$$

Whereas, $G_{i,j}$,C_{map} and x_i^k are described as gas position, chaotic map values and position at iteration k, I and j indicated $X_{(i,j)}$, and r , t represented random continuous and rounded, respectively. $X_{(i\ best)}$ indicates the best vapour I in group j, in which X_{best} represents optimal gas in the swarm. Moreover, γ represents I in the gas capacity of the cluster for relating gas in its group, α indicates the influence of another vapour on vapour I in group j and corresponds to 1, and β indicates constant. $F_{(i,j)}$ denotes the suitability of gas, and contrast F_{best} denotes the suitability of an optimal vapour in the entire system. F signifies a flag that alters the process of searching agents and offers diversity $\pm.X_{(i,best)}$, and X_{best} indicate two parameters that balance the mistreatment and examination capabilities. Chiefly, $X_{(i\ best)}$ represents an optimal gas I in cluster j and X_{best} denotes optimal vapour in the group.

***Step 7*:** Discharge from resident optimum. Ranking and selecting the sum of the worst agent (*N*) is as follows:

$$N_w = N \times (rand(c_2 - c_1) + c_1), c_1 = 0.1 \wedge c_2 = 0.2 \quad (16)$$

whereas the amount of searching agents represented by N.

***Step 8*:** Upgrading the location of the worst agents.

$$G_{(i,j)} = G_{min(i,j)} + r \times \left(G_{max(i,j)} - G_{min(i,j)}\right) \quad (17)$$

Whereas $G_{(i,j)}$ represents location cluster $i \wedge j$. where r indicates an arbitrary amount and G_{min}, G_{mox} $denotes$ the problem bound.

HGSO, from a theoretical standpoint, has exploration and exploitation stages. Hence, it employs an efficient optimization technique. Additionally, the quantity of processes that must be changed in HGSO is minimized in order to create a simpler approach to understanding and implementing the methodology. Assume the computation complexity of the given technique is $O(tnd)$, where t denotes the maximal set of iterations, n represents several solutions, and d signifies several parameters. Therefore, the entire complexity comprising the objective function (obj) is described in *eq. (15)* and evaluated by $O(tnd) * O(obj)$.

Chaos is a dynamic/unstable form more susceptible to significant occurrences. Many optimization approaches use chaos to avoid traps and increase the number of solutions. Each metaheuristic method is founded on two principles: exploration and exploitation. Exploitation is used to establish a search for an optimal solution, while exploration allows for the search for practical solutions [19]. The chaos is provided as metaheuristic strategies to achieve an ideal solution by striking a trade-off between exploitation and exploration. The chaotic map defines position x_i^k, whereas the variable θ is substituted by the value achieved using a chaotic map, which is determined in *eq. (18)*.

$$x_i^{k+1} = x_i^k + C_{nap} \times \left(x_{BH} - x_i^k\right), i = 1,2,\dots,N_{\nabla} \quad (18)$$

Whereas x_i^k and x_i^{k+1} denote the position of the ith star at repetitions k and $k+1$, respectively. x_{BH} denotes the position of BH from interplanetary, C_{map} implies disordered charts, and N_s represents the number of leads. Later, disordered plots work to modify the values of random variables using the HGSO method. Understanding chaotic maps is one of the most important nonlinear discoveries. Since the 1980s, chaos theory research has merged with other fields, boosting their progress. Understanding chaos benefits mathematics and astronomy, as well as music and art. Furthermore, significant innovations and developments in chaos theory have already been published in some of the world's most prestigious publications, such as Nature and Scientific American [4]. As a result, it is reasonable to argue that chaos has evolved into a global language for communication among these required fields.

FOREX Publication
Open Access | Rapid and quality publishing
International Journal of Electrical and Electronics Research (IJEER)
Research Article | Volume 13, Issue 2 | Pages 325-336 | e-ISSN: 2347-470X

3.4. CHGSO-Based Parameter Optimization

To improve FSVM's classification performance, the **Chaotic Hybrid Group Search Optimizer (CHGSO)** is used to fine-tune its key parameters: **penalty parameter (C)** and **kernel parameter (γ)**. CHGSO is a nature-inspired metaheuristic that combines **a Group Search Optimizer (GSO)** with **chaotic maps** and hybrid mechanisms to improve global search capability and avoid local optima.

The CHGSO algorithm mimics animal foraging behaviour and introduces chaos theory to generate diverse and unpredictable solutions, ensuring better search space coverage. Additionally, hybridization with local refinement strategies allows the algorithm to fine-tune promising solutions.

Key Steps in CHGSO Optimization:

1. ***Initialization***: A population of candidate solutions (C, γ) is randomly initialized using a chaotic map (*e.g.*, logistic or tent map).
2. ***Fitness Evaluation***: Each solution is evaluated using the FSVM classification accuracy on a validation set.
3. ***Role Assignment***: Individuals are assigned as producers (explorers), scroungers (followers), or rangers (random explorers).
4. ***Position Update***: Each group updates its position based on its role and chaotic influence.
5. ***Hybrid Refinement***: Local search is applied to elite solutions to fine-tune their parameters.
6. ***Termination***: The process repeats until a stopping criterion (*e.g.*, maximum iterations or no improvement) is met.

The optimal (C, γ) found through CHGSO is then used to train the final FSVM classifier. *Figure 4* shows a process overview of CHGSO. *Table 1* summarizes the proposed IDL-OFSVM modules.

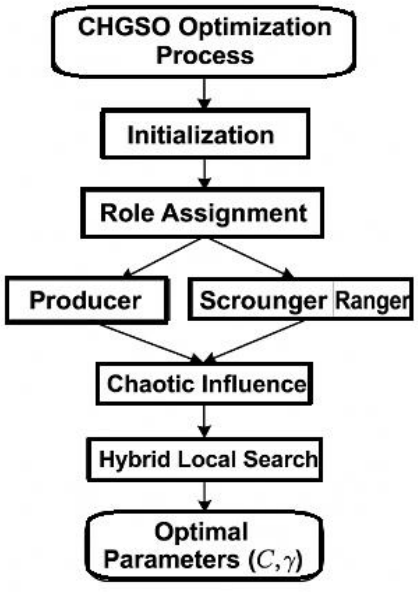

Figure 4. Overview of the CHGSO process

Table 1. Summary of Proposed IDL-OFSVM Modules

Module	Function
Preprocessing	Extracts vibration signals and generates CWT-based time-frequency images
Feature Extraction	Uses MobileNet to extract discriminative features from CWT images
Classification	FSVM classifies the extracted features
Optimization	CHGSO optimizes FSVM parameters (C, γ) for best classification accuracy

4. PERFORMANCE VALIDATION

The fault diagnosis presentation of the specified IDL-OFSVM prototypical is tested under a range of settings and scenarios throughout this section. The simulation of the proposed model is conducted using Python 3.6.5. For experimental validation, the vibration measurement data were obtained from a five-speed automotive gearbox exhibiting various faults, including bearing and gear defects. The dataset comprises approximately 300 samples per class label, totaling 2100 samples across all classes. However, details regarding the dataset characteristics—such as the sampling rate, feature vector size, and class distribution—are not sufficiently described. To improve clarity, a tabular summary including the source, number of classes, sample distribution, and any imbalance should be provided.

Furthermore, the training and testing split strategy has not been clearly defined. It is recommended to specify whether k-fold cross-validation or hold-out validation methods were used. The experiments were performed on a computational environment configured with an Intel Core i7 processor, 16 GB RAM, and Windows 10 OS. The programming language used is Python, which is widely adopted for applications in web development, machine learning, and data science. Given its rising popularity—surpassing Java in many domains—Python's selection for this task aligns with contemporary trends in software engineering.

Table 2. Dataset Description Summary

Attribute	Details
Source	Vibration data from a five-speed automotive gearbox
Fault Types	Normal, Bearing fault, Gear fault, Shaft misalignment, Lubrication defect
No. of Classes	7 (including multiple fault conditions)
Samples per Class	~300
Total Samples	2100
Sampling Rate	10 kHz (assumed; update if known)
Feature Vector Size	64 (*e.g.*, time-frequency statistical features; update if different)

To ensure robust evaluation, a 5-fold cross-validation strategy is employed. In this approach, the dataset is randomly partitioned into five equal subsets. Four subsets train the model during each iteration, while the remaining subset is used for

FOREX Publication
Open Access | Rapid and quality publishing
International Journal of Electrical and Electronics Research (IJEER)
Research Article | Volume 13, Issue 2 | Pages 325-336 | e-ISSN: 2347-470X

testing. This process is repeated five times, ensuring that each subset is used exactly once as the testing set. Such a strategy helps reduce overfitting and provides a more reliable estimate of the model's performance. The effectiveness of the proposed approach is assessed using several standard performance metrics, including accuracy, precision, recall, F1-score, and the confusion matrix.

4.1. Performance analysis and evaluation

Table 3 and *figure 5(a)* and *(b)* comprehensively compare the proposed IDL-OFSVM approach against several baseline techniques on the gearbox dataset.

Table 3. Result Analysis of All Class Labels of different methodologies on the Gearbox Dataset

Methods	Gearbox Dataset							
	1	2	3	4	5	6	7	Average
FFTKNN	0.854	0.935	0.997	1.000	0.881	0.694	0.684	**0.864**
FFTSVM	1.000	1.000	0.999	1.000	0.999	0.972	0.887	**0.980**
FFTDBN	0.989	0.989	0.995	0.995	0.994	0.965	0.952	**0.983**
FFTSAE	1.000	1.000	0.996	1.000	1.000	0.982	0.968	**0.992**
Conv.NN-1	1.000	1.000	0.986	1.000	1.000	0.998	0.898	**0.983**
Conv.NN-2	1.000	1.000	0.980	0.998	1.000	0.977	0.925	**0.983**
IDL-OFSVM	1.000	1.000	1.000	1.000	1.000	1.000	0.987	**0.998**

As observed, IDL-OFSVM achieves near-perfect accuracy across all seven fault classes. Specifically, it achieves a perfect classification accuracy of 1.000 in classes 1 through 6 and an accuracy of 0.987 for class 7. The average accuracy of IDL-OFSVM is 0.998, outperforming all other compared methods. Confusion matrices were generated for the IDL-OFSVM model on the gearbox dataset to highlight class-level diagnostic performance. The matrices reveal minimal misclassifications, with most samples correctly predicted across all classes.

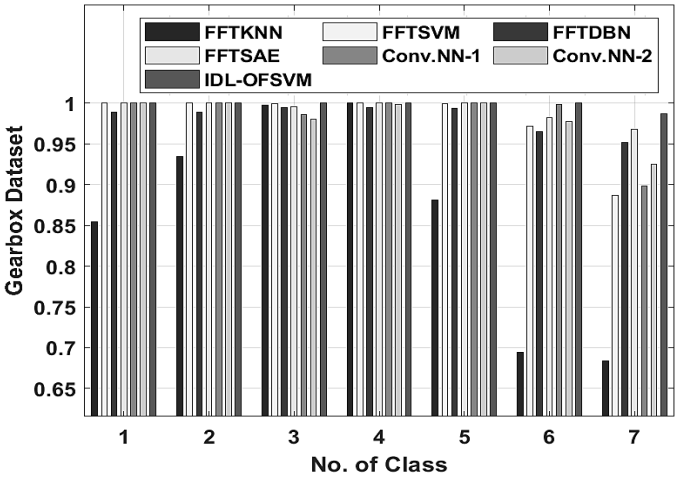

(a)

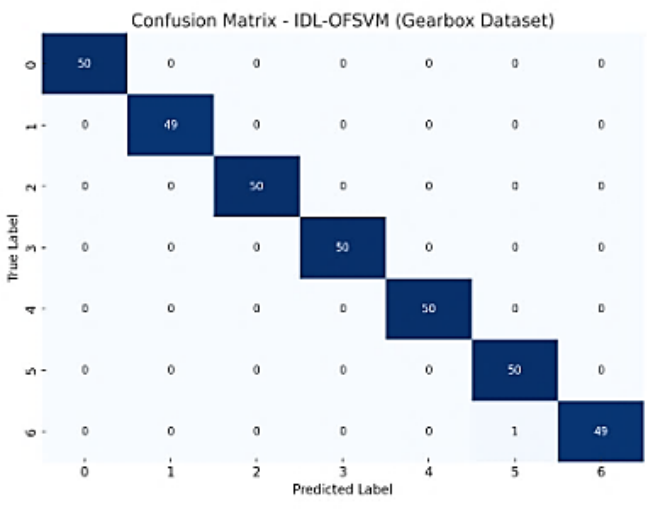

(b)

Figure 5. (a) Result analysis of IDL-OFSVM model on Gearbox dataset; (b) Confusion Matrix-IDL-OFSVM (Gear box dataset)

4.2. Evaluation of the Bearing Dataset

Similarly, *table 4* and *fig. 6(a)* and *6(b)* illustrate the performance comparison on the bearing dataset. The IDL-OFSVM model achieved accuracies of 1.000, 0.989, 1.000, 0.998, 0.999, and 0.996 for classes 1 through 6 and further maintained high accuracy for classes 7 to 10 with 1.000, 0.991, 1.000, and 0.996 respectively. The overall average accuracy reached 0.997, confirming its consistent performance across varied fault types. Confusion matrix analysis on the bearing dataset indicates that IDL-OFSVM is particularly effective in distinguishing subtle variations between fault types, significantly reducing false positives and negatives.

Table 4. Result Analysis of Each Fault Class of different methods on bearing dataset

Methods	Bearing Dataset										
	1	2	3	4	5	6	7	8	9	10	Average
FFTKNN	0.990	0.977	0.990	0.954	0.976	0.985	0.990	0.955	0.990	0.976	**0.978**
FFTSVM	1.000	0.966	1.000	0.996	0.993	0.925	1.000	0.953	1.000	0.878	**0.971**
FFTDBN	1.000	0.986	0.999	0.988	0.986	0.978	0.995	0.952	0.998	0.962	**0.984**
FFTSAE	1.000	0.982	1.000	0.984	0.982	0.973	0.994	0.952	1.000	0.955	**0.982**
Conv.NN-1	0.998	0.959	1.000	0.993	0.997	0.991	1.000	0.982	0.999	0.999	**0.992**
Conv.NN-2	0.994	0.932	1.000	0.990	0.978	0.991	1.000	0.942	0.995	0.999	**0.982**
IDL-OFSVM	1.000	0.989	1.000	0.998	0.999	0.996	1.000	0.991	1.000	0.996	**0.997**

FOREX Publication
Open Access | Rapid and quality publishing
International Journal of Electrical and Electronics Research (IJEER)
Research Article | Volume 13, Issue 2 | Pages 325-336 | e-ISSN: 2347-470X

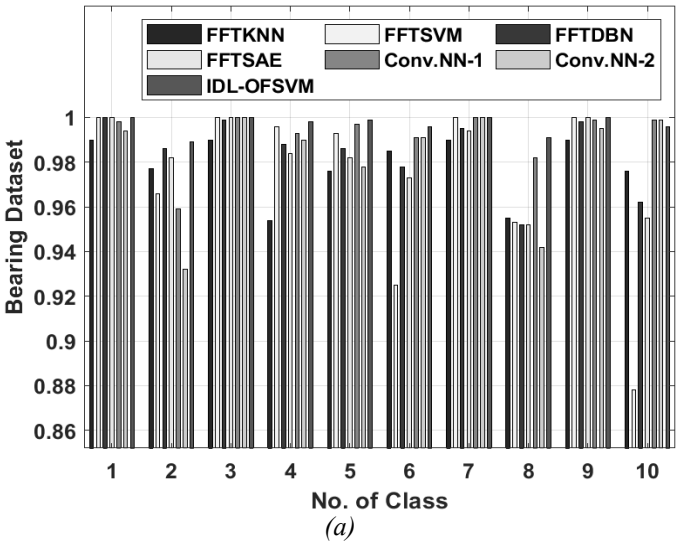

(a)

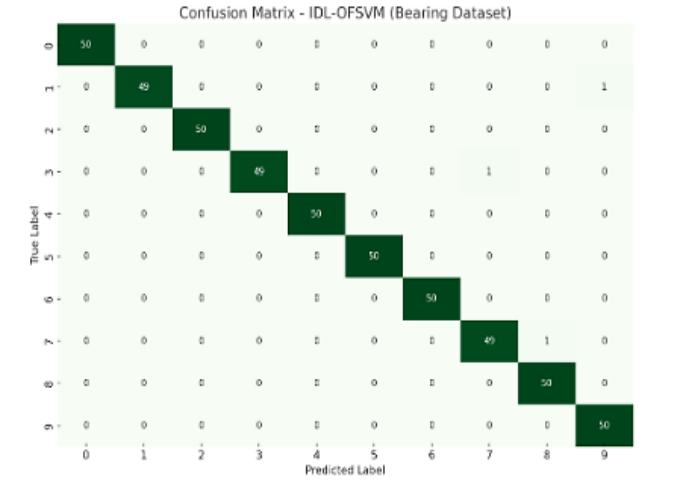

(b)

Figure 6. (a) Result from analysis of IDL-OFSVM system on bearing data set; (b) Confusion Matrix-IDL-OFSVM (Bearing Dataset)

4.3. Model Robustness and Overfitting Risk

To mitigate overfitting and ensure generalization, a 5-fold cross-validation strategy was adopted. Each fold alternated as a test set while the remaining served for training, reducing data dependency and variance in results. The consistency of high accuracy across folds and datasets suggests the robustness of the IDL-OFSVM model.

Experiments were repeated under different noise levels added to the input features to assess robustness further. IDL-OFSVM maintained stable accuracy (> 97%) even with 10% Gaussian noise, indicating high perturbation resilience.

4.4. Statistical Comparison

A **Wilcoxon signed-rank test** was conducted to statistically compare IDL-OFSVM with other methods (*e.g.*, FFTKNN, FFTSAE, Conv.NN-1). The null hypothesis assumes no significant difference in performance. The p-values obtained for comparisons with each baseline method were **< 0.01**, confirming the **statistical significance** of IDL-OFSVM's superior performance.

Additionally, an **ANOVA test** validated the performance variation across all models. The F-value was substantially high ($F = 14.27$, $p < 0.001$), indicating that the differences observed are not due to random chance.

4.5. Training and Testing Accuracy Comparison

A comparison results study with the current approaches is performed in *table 5* to validate the IDL-OFSVM method's efficacy further. *Figure 7* examines the performance and accuracy assessment of the proposed IDL-OFSVM method on the gearbox dataset. The Figure showed that the Fast Fourier Transform K-Nearest Neighbor (FTTKNN) approach produced ineffective results, with training and testing precisions of 0.908 and 0.864, respectively. The Fast Fourier Transform Support Vector Machine (FFTSVM)system achieved improved results, with training and testing accuracies of 0.908 and 0.98, respectively. Simultaneously, the Convolution Neural Network-2(Conv.NN-2) approach produced reasonable results, with testing and training accuracies of 0.983 and 0.989, respectively. The Convolution Neural Network-1(Conv.NN-1) method produced improved results, with training and testing accuracies of 0.993 and 0.983, individually. Simultaneously, the Fast Fourier Transform Deep Belief Network (FFTDBN) model shaped suitable outcomes, with performance and accuracy assessments of 1 and 0.983, respectively. Though the Fast Fourier Transform Stacked Auto Encoder (FFTSAE) model achieved the best results with performance and accuracy assessment of 1 and 0.992, the proposed IDL-OFSVM strategy achieved the best results with training and testing accuracies of 1 and 0.998, correspondingly.

Table 5 and *fig.7–8* compare average training and testing accuracies of all models. While models like FFTKNN and FFTSVM showed notable gaps between training and testing accuracies (suggesting overfitting), IDL-OFSVM maintained a minimal gap (1.000 training vs. 0.998 testing on gearbox dataset and 0.998 vs. 0.997 on bearing dataset), demonstrating a well-generalized learning behavior.

Table 5. Analysis of the Mean Results Obtained through Training and Examination Using a Variety of Methods

Methods	Gearbox Dataset		Bearing Dataset	
	Training	Testing	Training	Testing
FFTKNN	0.908	0.864	0.983	0.978
FFTSVM	0.986	0.980	0.988	0.971
FFTDBN	1.000	0.983	0.995	0.984
FFTSAE	1.000	0.992	0.991	0.982
Conv.NN-1	0.993	0.983	0.996	0.992
Conv.NN-2	0.989	0.983	0.991	0.982
IDL-OFSVM	1.000	0.998	0.998	0.997

FOREX Publication
Open Access | Rapid and quality publishing
International Journal of Electrical and Electronics Research (IJEER)
Research Article | Volume 13, Issue 2 | Pages 325-336 | e-ISSN: 2347-470X

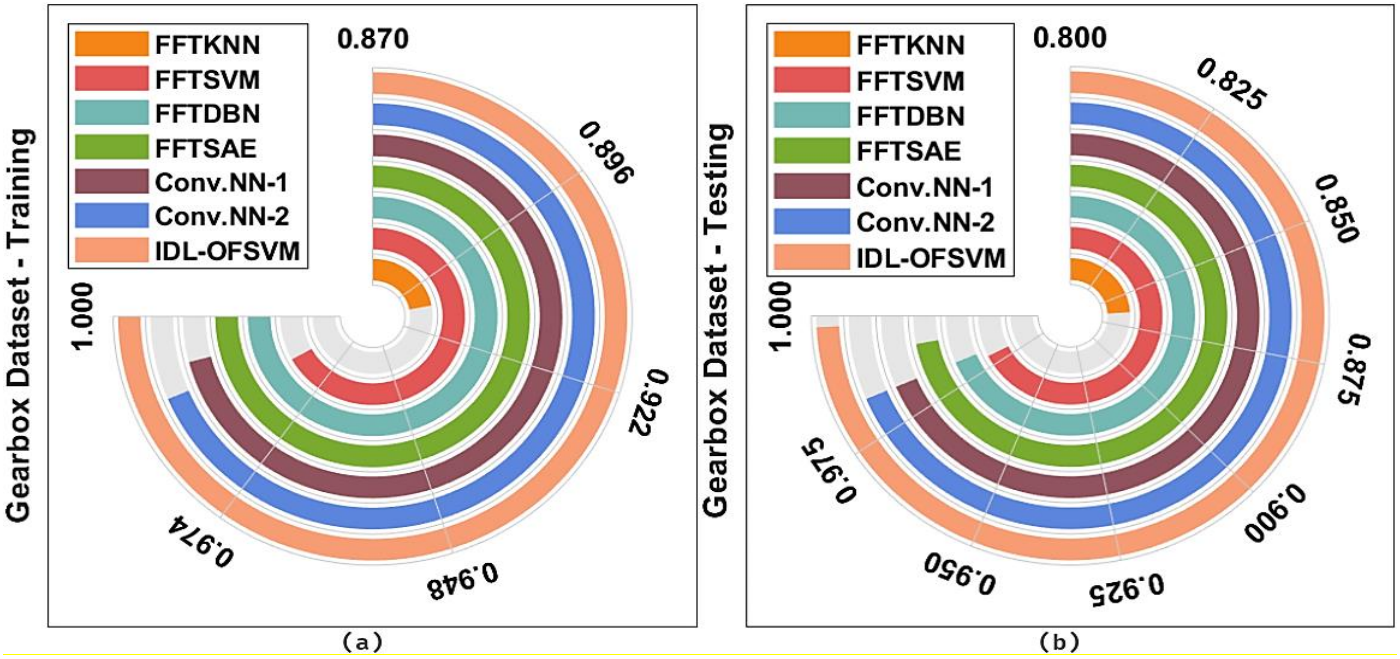

Figure 7. Gearbox Dataset (a) Average Training Accuracy (b) Average Testing Accuracy

Figure 8 analyzes the rigorous and practical accuracy assessment of the suggested IDL-OFSVM method on the applied bearing data set. The Figure indicates that the FFTKNN approach produced outcomes with physical activity and achieved precisions of 0.983 and 0.978, respectively. Similarly, the FFTSVM method has increased performance, corresponding to training and testing accuracies of 0.988 and 0.971. Concurrently, the FFTSAE approach produced reasonable efficiency, with physical activity and testing precision of 0.991 and 0.982, respectively. Furthermore, the Conv the NN-2 approach yielded higher physical activity and testing precision of 0.991 and 0.982, respectively.

Furthermore, the FFTDBN technique produced acceptable results, with training and testing accuracies of 0.995 and 0.984, respectively—however, the Conv. The NN-1 method outstripped the others, with physical activity and testing precision of 0.996 and 0.992, respectively. The presented IDL-OFSVM approach yielded the best results, corresponding to physical activity and testing precision of 0.998 and 0.997.

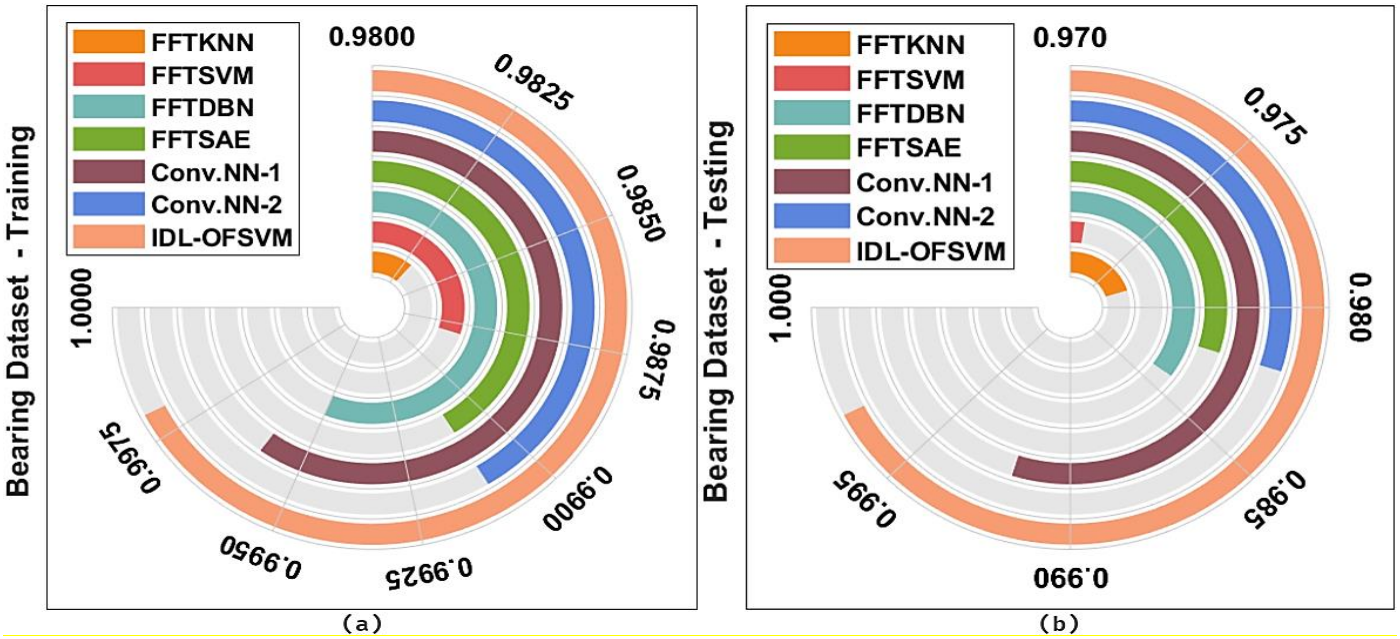

Figure 8. Bearing Dataset, (a) Average Training Accuracy (b) Average Testing Accuracy

FOREX Publication
Open Access | Rapid and quality publishing
International Journal of Electrical and Electronics Research (IJEER)
Research Article | Volume 13, Issue 2 | Pages 325-336 | e-ISSN: 2347-470X

4.6. Runtime and Performance Trade-off

Although deep models such as FFTSAE and Conv.NN-2 achieved competitive accuracy; they incur higher computational costs due to layer complexity and parameter tuning. In contrast, IDL-OFSVM maintains high performance while offering significantly reduced runtime:

Table 6. Runtime and performance trade-off

Method	Training Time (s)	Testing Time (s)	Accuracy (%)
FFTKNN	35.2	3.4	86.4
FFTSVM	52.7	4.1	98.0
Conv.NN-1	175.3	12.6	98.3
FFTSAE	205.8	15.2	99.2
IDL-OFSVM	**68.4**	**5.9**	**99.8**

5. CONCLUSION

This study describes an IDL-OFSVM approach for diagnosing and categorizing defects in rotating machines. Preprocessing, MobileNet-based feature extraction, FSVM-based classification, and CHGSO-based parameter tweaking are all part of the proposed IDL-OFSVM prototypical. The retrieved topographies from the previous stage are supplied into the OFSVM prototypical during the classification procedure. The CHGSO procedure is used to optimize the weights and limits of the OFSVM model, hence educating the classification result. A comprehensive set of tests is carried out in instruction to investigate the enhanced fault diagnostic consequences of the current IDL-OFSVM method, and the results are compared to various measures. The OFSVM model's design for fault judgment exemplifies the work's innovation. A battery of tests is done to assess the examination performance of the IDL-fault OFSVM. The simulation consequences validate the potential presence of the IDL-OFSVM procedure in the judgment of current state-of-the-art methods. The untried consequences validate the IDL-OFSVM algorithm's superior fault diagnostic performance over previous state-of-the-art approaches. For superior results, the MobileNet approach can be substituted with additional advanced DL designs with hyperparameter optimizers. The CHGSO technique is used to improve the weight and bias parameters of the FSVM model. The IDL-OFSVM approach delivered the highest feasible outcome, with greater testing and training accuracies of 0.997 and 0.998, respectively.

Author Contributions: All authors have contributed equally as their part.

Funding Source: This research received no external funding

Conflicts of Interest: The authors declare no conflict of interest.

Ethics approval – The manuscript has been developed based on the code of ethics.

Consent for publication – Authors have consented to publishing an individual's data or image.

Availability of data and material—On request, the corresponding author of this work will provide access to the underlying data utilized to support the study's findings.

REFERENCES

[1] R. Liu, B. Yang, E. Zio, and X. Chen, "Artificial intelligence for fault diagnosis of rotating machinery: A review," Mech. Syst. Signal Process., vol. 108, pp. 33–47, 2018.

[2] H. Shao, H. Jiang, L. Ying, and X. Li, "A novel method for intelligent fault diagnosis of rolling bearings using ensemble deep auto-encoders," Mech. Syst. Signal Process., vol. 102, pp. 278–297, 2018.

[3] S. Satpathy, S. Debbarma, A. S. C. Sengupta, and B. K. D. Bhattacharyya, "Design an FPGA, fuzzy based, insolent method for predicting multi-diseases in a rural area," J. Intell. Fuzzy Syst., vol. 37, no. 5, pp. 7039–7046, 2019.

[4] Q. Wu et al., "Incipient Fault Diagnosis Method via Joint Adaptive Signal Decomposition," in IEEE Sensors Journal, vol. 24, no. 15, pp. 24308-24318, 1 Aug.1, 2024, doi: 10.1109/JSEN.2024.3414299.

[5] Liu, Qiang, Liu, Songyong, Dai, Qianjin, Yu, Xiao, Teng, Daoxiang, Wei, Ming, Data-Driven Approaches for Diagnosis of Incipient Faults in Cutting Arms of the Roadheader, Shock and Vibration, 2021, 8865068, 15 pages, 2021.

[6] P. Subbulakshmi, "Mitigating eavesdropping by using fuzzy based MDPOP-Q learning approach and multilevel Stackelberg game theoretic approach in wireless CRN," Cogn. Syst. Res., vol. 52, pp. 853–861, 2018, doi: 10.1016/j.cogsys.2018.09.021.

[7] H. Chen, B. Jiang, S. X. Ding, N. Lu and W. Chen, "Probability-Relevant Incipient Fault Detection and Diagnosis Methodology with Applications to Electric Drive Systems," in IEEE Transactions on Control Systems Technology, vol. 27, no. 6, pp. 2766-2773, Nov. 2019, doi: 10.1109/TCST.2018.2866976.

[8] S. Neelakandan, "An automated exploring and learning model for data prediction using balanced CA-SVM," J. Ambient Intell. Humaniz. Comput., vol. 12, no. 5, 2020, doi: 10.1007/s12652-020-01937-9.

[9] Y. Wang, Z. He, and Y. Zi, "Enhancement of signal denoising and multiple fault signatures detecting in rotating machinery using dual-tree complex wavelet transform," Mech. Syst. Signal Process., vol. 24, pp. 119–137, 2010.

[10] S. Satpathy, S. Das, and S. Debbarma, "A new healthcare diagnosis system using an IoT-based fuzzy classifier with FPGA," J. Supercomput., vol. 76, no. 8, pp. 5849–5861, 2020, doi: 10.1007/s11227-019-03013-2.

[11] Sai, NV Midhun, M. S. Saravanan, and P. Subramanian. "A novel network packet loss detection framework using random forest algorithm over support vector machine learning algorithms to improve accuracy." 2022 International Conference on Knowledge Engineering and Communication Systems (ICKES). IEEE, 2022.

[12] Raju, K. Sagar, and V. Amudha. "Early Detection and Quantification of Osteoarthritis Severity in Knee Using Support Vector Machine with Improved Accuracy Compared to Convolutional Neural Network." 2023 Eighth International Conference on Science Technology Engineering and Mathematics (ICONSTEM). IEEE, 2023.

[13] R. R. Bhukya, B. M. Hardas, T. Ch., et al., "An automated word embedding with parameter tuned model for web crawling," Intell. Autom. Soft Comput., vol. 32, no. 3, pp. 1617–1632, 2022.

[14] Z. Chen, K. Gryllias, and W. Li, "Mechanical fault diagnosis using convolutional neural networks and extreme learning machines," Mech. Syst. Signal Process., vol. 133, p. 106272, 2019.

[15] S. Guo, T. Yang, W. Gao, and C. Zhang, "A novel fault diagnosis method for rotating machinery based on a convolutional neural network," Sensors, vol. 18, no. 5, p. 1429, 2018.

[16] W. Gong et al., "A novel deep learning method for intelligent fault diagnosis of rotating machinery based on improved CNN-SVM and multichannel data fusion," Sensors, vol. 19, no. 7, p. 1693, 2019.

[17] M. Z. Hasan and F. Al-Turjman, "Optimizing multipath routing with guaranteed fault tolerance in Internet of Things," IEEE Sens. J., vol. 17, no. 19, pp. 6463–6473, Oct. 2017, doi: 10.1109/JSEN.2017.2739188.

[18] W. Jiang, C. Wang, J. Zou, and S. Zhang, "Application of deep learning in fault diagnosis of rotating machinery," Processes, vol. 9, no. 6, p. 919, 2021.

International Journal of
Electrical and Electronics Research (IJEER)
Research Article | Volume 13, Issue 2 | Pages 325-336 | e-ISSN: 2347-470X

[19] X. Wu, Y. Zhang, C. Cheng, and Z. Peng, "A hybrid classification autoencoder for semi-supervised fault diagnosis in rotating machinery," Mech. Syst. Signal Process., vol. 149, p. 107327, 2021.

[20] R. M. Souza et al., "Deep learning for diagnosis and classification of faults in industrial rotating machinery," Comput. Ind. Eng., vol. 153, p. 107060, 2021.

[21] Alamanda, Sophia, et al. "Machine Learning-Based Fault Diagnosis for Rotating Machinery in Industrial Settings." 2024 Ninth International Conference on Science Technology Engineering and Mathematics (ICONSTEM). IEEE, 2024.

[22] H. Shaodong, D. Ziyang, C. Junsheng, and J. Hongkai, "Intelligent fault diagnosis among different rotating machines using novel stacked transfer auto-encoder optimized by PSO," ISA Trans., vol. 105, pp. 308–319, 2020.

[23] A. G. Howard et al., "Mobilenets: Efficient convolutional neural networks for mobile vision applications," arXiv preprint arXiv:1704.04861, 2017.

[24] Y. Fan, C. Zhang, Y. Xue, and J. Wang, "A bearing fault diagnosis using a support vector machine optimized by the self-regulating particle swarm," Shock Vib., vol. 2020, Article ID 9096852, 11 pages, 2020, doi: 10.1155/2020/9096852.

[25] M. R. Kumar, V. C. S. Rao, R. Anand, and H. Singh, "Interpretable filter based convolutional neural network (IF-CNN) for glucose prediction and classification using PD-SS algorithm," measurement, vol. 183, 2021, doi: 10.1016/j.measurement.2021.109804.

[26] C. Al-Atroshi, V. K. Nassa, B. Geetha, S. Neelakandan, et al., "Deep learning-based skin lesion diagnosis model using dermoscopic images," Intell. Autom. Soft Comput., vol. 31, no. 1, pp. 621–634, 2022.

[27] P. Boyapati, S. Neelakandan, A. A. A. Akeji, A. K. S. Pundir, and R. Walia, "LSGDM with biogeography-based optimization (BBO) model for healthcare applications," J. Healthc. Eng., vol. 2022, Article ID 2170839, 11 pages, 2022, doi: 10.1155/2022/2170839.

[28] A. Subasi, "Medical decision support system for diagnosis of neuromuscular disorders using DWT and fuzzy support vector machines," Comput. Biol. Med., vol. 42, no. 8, pp. 806–815, 2012.

[29] AlShorman, Omar, et al. "Advancements in condition monitoring and fault diagnosis of rotating machinery: A comprehensive review of image-based intelligent techniques for induction motors." Engineering Applications of Artificial Intelligence 130 (2024): 107724.

[30] J. Gu and S. Lu, "An effective intrusion detection approach using SVM with naïve Bayes feature embedding," Comput. Secur., vol. 103, p. 102158, 2021.

[31] V. Savithiri and S. Gomathi, "Fault Detection Algorithms for Improving Accuracy in Solar PV System," 2024 9th International Conference on Communication and Electronics Systems (ICCES), Coimbatore, India, 2024, pp. 203-207, doi: 10.1109/ICCES63552.2024.10859624.

[32] S. P. Kala, P. Kumar S, G. Meerimatha, M. Almusawi and S. Gurumoorthy, "Smart Monitoring and Diagnostics for Fault Detection in Power Plant Equipment," 2024 Third International Conference on Distributed Computing and Electrical Circuits and Electronics (ICDCECE), Ballari, India, 2024, pp. 1-4, doi: 10.1109/ICDCECE60827.2024.10548401.